Research Article Vol. 30, No. 5 / 28 Feb 2022 / Optics Express 7017
Optics EXPRESS

Nano-antenna array for high efficiency sunlight harvesting

MICHELE MIDRIO,[1] LUCA PIERANTONI,[2] STEFANO BOSCOLO,[1] DAVIDE TRUCCOLO,[1] AND DAVIDE MENCARELLI[2,*]

[1] *Università degli Studi di Udine, Departimento Politecnico di Ingegneria e Architettura, Via delle Scienze 206, 33100 Udine, Italy*
[2] *Università Politecnica delle Marche, Department of Information Engineering, Via Brecce Bianche 12, 60131 Ancona, Italy*
[*] *d.mencarelli@univpm.it*

Abstract: Solar rectennas are promising devices for energy harvesting. Capability of rectennas to convert incident light into useful energy depends on the antenna efficiency, that is the ratio between the power transferred to the load vs the incoming power. In this work, we first emphasize that for the efficiency to be calculated accurately, antennas need to be treated as receiving devices, not as transmitting ones. Then, we propose an arrangement of antennas that differs from those published so far in three respects: (1) the proposed arrangement is formed by an array of nano-antennas with sub-wavelength inter-element spacing, (2) it comprises a reflecting mirror, and (3) it allows for dual polarization operation. Through numerical simulations, we show that the small lattice pitch we use is responsible for frequency flattening of the lattice impedance over the whole solar spectrum, eventually allowing for excellent matching with the antennas' loads. Also, the small pitch allows for a smooth dependence of the receiving efficiency on the angle of incidence of sunlight. Finally, we show numerically that the reflecting mirror also allows for an almost complete cancellation of light scattered by the receiving antennas. The final result is a polarization insensitive receiving theoretical efficiency larger than 70% over the whole 300-3000 nm spectral range, with a less than 10% energy wasting due to back-scattering of sunlight.

1. Introduction

The increase of renewable energy [1] in the global energy mix [2] and of the energy efficiency [3] are among the goals that United Nations (UN) have adopted as part of the 2030 Agenda for Sustainable Development [4].

Energy efficiency is any means for measuring the energy-expenditure required to achieve a given benefit [3]. Renewable energies are energies obtained from natural and inexhaustible resources which can continually self-regenerate [1]. Sunlight is one of the major available sources of renewable energy [5]. Two technologies are currently used to produce electricity from sunlight [6]: photovoltaics [7] and concentrating solar power [8]. In photovoltaics, sunlight is converted into electricity through the photo-electric effect [9]. A record lab cell efficiency of 26.7% was demonstrated for mono-crystalline silicon [10], decreasing to 24.4% for multi-crystalline silicon wafer-based technology. Using more complex and costly quadruple junctions [11], an efficiency as large as 44.7% was obtained. A complete list of record-performance obtained with different technologies can be found in [12].

Concentrating solar power exploits reflectors to focus sunlight on small areas and generate steam for use in thermal electric plants [8]. A nearly 47% record solar to electric conversion efficiency was obtained under southern Egypt climate [13]. Photovoltaics exploit a physical effect related to the quantization of light energy. However, alternative mechanisms for harvesting of sunlight may be envisaged by taking avantage of the wave nature of sunlight. In this respect,

#450020 https://doi.org/10.1364/OE.450020
Journal © 2022 Received 30 Nov 2021; revised 20 Jan 2022; accepted 20 Jan 2022; published 16 Feb 2022

Optics EXPRESS

conversion of light into electrical power can be obtained by realizing a so-called rectenna [14], that is an antenna connected to a rectifying diode. Originally, rectennas were developed to feed high amplitude atmospheric platforms through microwave beams pointed at the vehicles [15]. Later on, the idea was transferred to much higher frequencies with the aim of extracting DC power from sunlight [16].

In contrast to photovoltaics that have a theoretical maximum efficiency limit around 33% for single junction cells [17], raising to a theoretical maximum of 68% in an infinite stack of solar cell under 1-sun illumination, and further up to 86% for concentrated solar light [18], the efficiency of rectennas is solely limited by thermodynamic considerations and can be larger than 80% [19]. Such efficiencies have been experimentally demonstrated at microwaves [20]. Also, an efficiency as large as 58% has been demonstrated at 897 GHz [21], but not yet for visible or infrared light.

For many years, rectification of sunlight was almost exclusively an academic field of research. Commercial implementation of solar rectifiers clashed because of two main issues. First, typical dimensions of antennas for solar harvesting are in the order of fractions of the wavelengths they aim at receiving [22,23]. This in turn requires fabrication processes that can reliably and reproducibly realize nanometric structures. Second, even the fastest electronic diode cannot operate at frequencies of visible or near IR light [24,25]. Metal-Insulator-Metal (MIM) diodes were proposed for rectifying THz waves [26,27]. However, when the capacity of those diodes is combined with the intrinsic resistance of any receiving antenna, time constant too long to harvest sunlight [28] is typically obtained. In fact, experimental attempts to rectify visible light through MIM didoes resulted in rather limited conversion efficiencies [29]. In recent years, the fast development of nanotechnology and the discovery of graphene [30] have changed the perspectives of sunlight rectification [31]. Technologies to obtain the extremely tiny dimensions needed in nanoantennas are at hand: 7-nm node is expected to be fully operative by 2021, and 1.4nm by 2029 [32]. As per rectification, the large mean-free path length of charges in graphene [33] opened up the way to geometrical diodes [34,35]. Those are diodes where asymmetry comes from the physical shape of the device. Rectennas working at frequencies as large as 28 THz have already been demonstrated with this kind of diode [34], though no experimental results are available yet at visible and IR wavelengths. Whatever the technology for manufacturing nano-antennas and the choice of the rectifying diode will be, the final efficiency of any rectenna will consist of two parts [36]: 1) the receiving efficiency by which the power of sunlight is transferred to the antenna load (that is: to the diode) and 2) the efficiency by which the captured light is transformed to DC power.

In the present paper, we do not discuss on the second of the above points and we show that if the impedance of the diode approaches a purely resistive value, the layout of optical antennas we propose may theoretically provide a remarkable receiving efficiency as large as 71%. As per the physical manufacturability of a purely resistive diode, we observe that MIM are clearly not adequate structures. Whereas, geometric or ballistic diodes could be promising candidates. Indeed, it was shown that in these structures "*the electrical contacts are laterally separated rather than placed on the surface and the back side (substrate), the parasitic capacitance between contacts is substantially lower than in a conventional vertical device of the same size*" (the text is quoted literally from Ref. [37], see also [38,39])". After having thoroughly discuss the ideal case of a purely resistive load, we will numerically evaluate to what extent a capacitive part in the diode impedance reduces the receiving efficiency of the proposed antennas layout.

We have highlighted the term "*receiving efficiency*", that is the ratio between the optical power transferred to the load to the power of the incoming sunlight because we believe that receiving efficiency is the correct way of measuring performance of antennas in the field of sunlight harvesting. Readers will notice that this way of measuring the antenna performance differs from those used in previously published papers, where antennas where regarded as transmitting devices. For instance, Vandenbosch and Ma thoroughly investigated performance of linear dipole

Optics EXPRESS

antennas [40]. They showed a 65% transmitting efficiency when averaging over the whole Planck's blackbody radiation curve [40]. In a companion paper, the same Authors also showed that the efficiency is 54% when loss in the antenna and a second order polynomial rectifier impedance model is included in the model [36]. More recently, Zhao and coauthors claimed an 80% efficiency with a nanospiral antenna [41] (but with limitation in terms of polarization, as it is remarked later).

Despite the existing literature, there are several reasons why a further study on the antenna efficiency is worth, at least in our opinion:

1. existing studies considered single isolated antennas only. A real solar panel aiming at efficient sunlight harvesting will certainly contain an array of antennas instead of a single isolated one. In addition, antennas in the array will be closely packed for efficient exploitation of the available space; coupling between neighboring antennas likely changes the efficiency and should hence be included in the analysis;

2. also, existing studies mostly considered antennas in free space (or, at most, over a dielectric slab). In our opinion, in any realistic solar panel, a metallic reflector will be placed below the antennas both to enlarge gain in the broadside direction on top of the antennas, and to possibly increase mechanical stability of the device while also providing an electrical contact for collecting rectified currents;

3. the behavior of antennas should be stable with respect to the angle of incidence of the incoming sunlight; certainly, this is not the case for isolated dipole antennas, nor for spirals;

4. dual polarization antennas will be needed as sunlight is not polarized. In this respect too, dipoles certainly do not match the requirement. Nor do it spirals, which receive either a left or a right handed circular polarization, not both.

In the present paper we address all the points above by considering the periodically loaded surface schematically depicted in the top panel of Fig. 1. An array of optical antennas is arranged in a square lattice with pitch Λ. Antennas (violet shapes in the figure) are metallic square patches with lateral dimension L_A and thickness H_A, placed on top of a dielectric substrate with thickness H_{diel} and relative dielectric constant ϵ_{diel}. A layer of metal beneath the dielectric substrate acts as a back-reflector. Red rectangles in the figure are loads, possibly diodes allowing for THz rectification. It is remarked that loads are only seen as resistive loads in the present paper, and no speculations are made on their physical shape or working principle, nor on their rectifying capabilities. The bottom panel of the figure shows a top view of the structure.

2. Some distinctive features of the periodically loaded surface in Fig. 1

In this Section we discuss some distinctive features of the periodically loaded surface in Fig. 1.

Coupling between neighboring antennas. Coupling between neighboring antennas in an array is generally regarded as a detrimental effect that eventually causes decay of performance [42]. Luckily, this is not always the case. Realizing an array of strongly coupled antennas may indeed allow to obtain performance stability both with respect to frequency and to angle of incidence of incoming light [43,44,45].

As it was shown by B. A. Munk in Refs. [43,45], the interplay between the presence of dielectrics and of a back-reflector along with a small inter-element spacing in an array of antennas can help providing a stable resonant frequency over the angle of incidence. In fact, getting antennas in the lattice close to each other brings to an almost constant current distribution over the plane that contains the antennas. This way, the plane becomes similar to an aperture antenna with a continuous current, which is the ideal situation for a broadband radiator [46]. Also, the imaginary part of the mutual impedance between antennas in the lattice starts canceling each

Optics EXPRESS

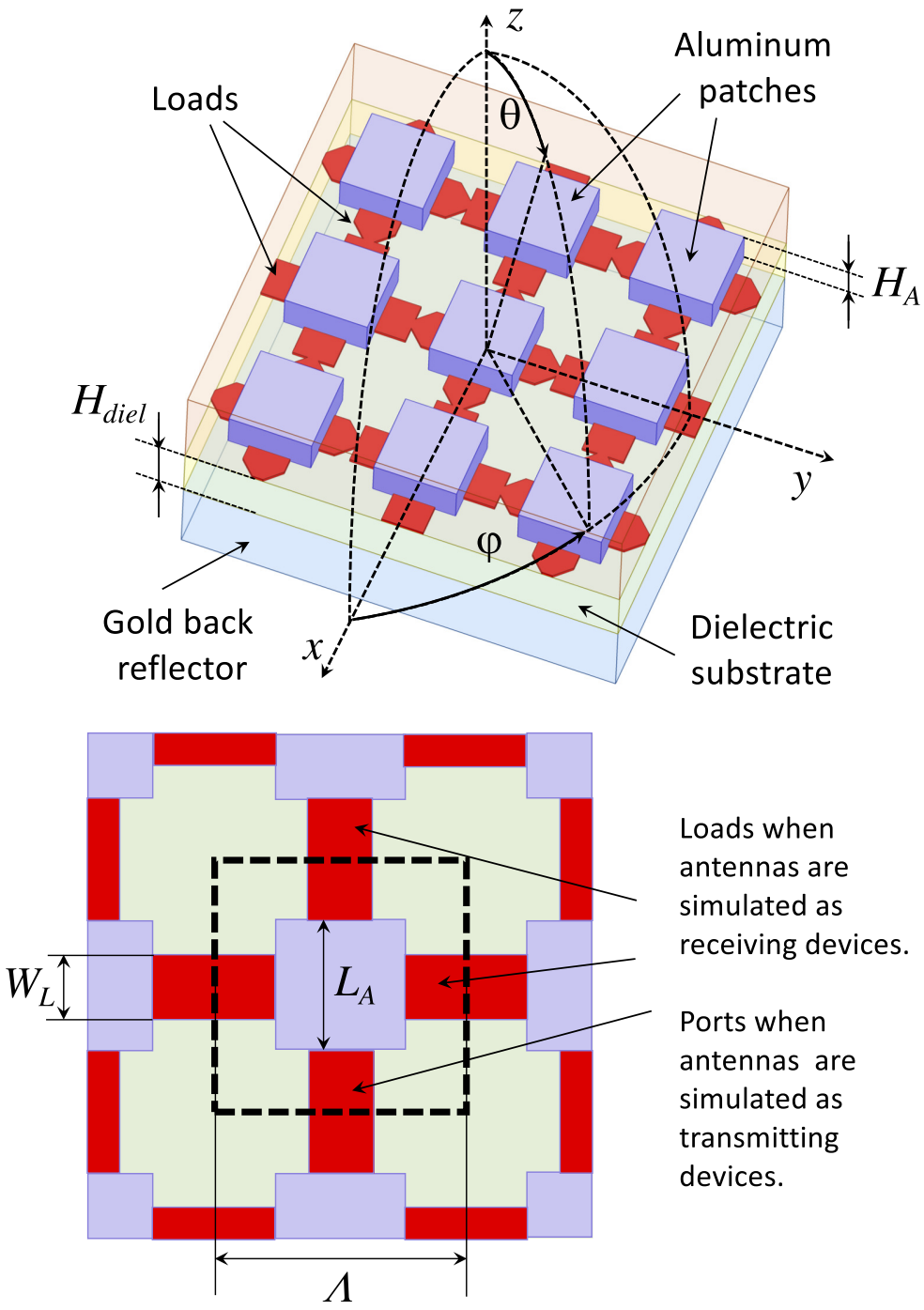

Fig. 1. Top: schematic diagram of the periodically loaded surface considered in the present work. Bottom: top view of the unit cell in the squared array.

other as one moves away from the reference element provided that the interelement spacings are small (<0.4λ), eventually leading to less stored energy between the antennas, and therefore to smaller imaginary components of the overall antenna impedance. The reader may find a detailed

Optics EXPRESS

explanation of the bandwidth enhancement that can be realised with small inter-element spacing arrays in Sections 3, 4, 5 and 12 of Chapter 6 of Ref. [45] as well as in Appendices B and D of the same book.

Figure 2 confirms the above statement and shows the benefit of using an array of antennas instead of a single one in terms of antenna impedance in the lattice of Fig. 1. The figure refers to a lattice where squared aluminum antennas with lateral size L_A = 72nm and thickness H_A = 90 nm are placed on a lattice with pitch Λ = 140nm. The substrate layer relative permittivity and thickness are ϵ_{diel}=2.25, and H_{diel} = 71 nm, respectively. In these simulations, antennas are made of aluminum, and the reflector is an 80 nm thick layer of gold. Complex dielectric constants with parameters taken from Ref. [47] have been considered in these simulations for both aluminum and gold. In the left panel of the figure, we show the real (black solid line) and imaginary (red solid line) input impedance between any couple of neighboring antennas in the lattice. On the right side of the figure, the curves refer to the case of a single antenna, i.e. an antenna formed by two isolated aluminum squares. Input impedance is the impedance measured at the the antenna terminals (for a single isolated antenna), or between any couple of neighbouring antennas (for the lattice) when antennas are used as transmitting devices. The figure confirms that the lattice stabilizes the antenna impedance. When the antennas are used as receiving devices, this allows for an easier matching to the load impedance.

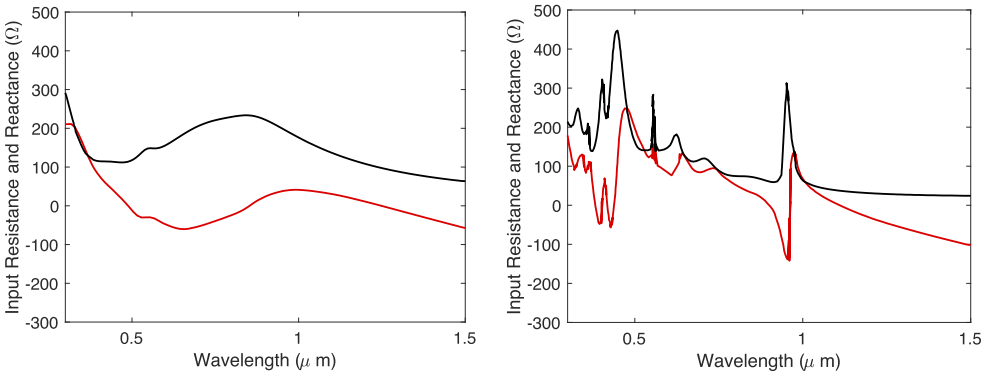

Fig. 2. Input impedance (black: real part, read: imaginary part) of aluminum squared antennas. Left panel: impedance for antennas in a lattice. Right panel: impedance for a single isolated antenna. Input impedance is the impedance measured at the the antenna terminals (for a single isolated antenna), or between any couple of neighbouring antennas (for the lattice) when antennas are used as transmitting devices.

Back-reflector. An even more important feature of the periodically loaded surface in Fig. 1 is the presence of the back-reflector that allows to increase the amount of power delivered to the antennas' loads, and therefore the receiving efficiency. To better clarify the crucial role of the back-reflector, it is worth recalling two general properties of receiving antennas.

- Property 1. The receiving area of an array of antennas with no ground-plane is, at most, half its physical size [48]. Let us see the practical implications of this property. Suppose an incident wave impinges on an array of ideally lossless antennas closed on perfectly matched loads. The above property means that, at best, the array can transfer half of the incident power to its loads. The remaining half is "lost" to scattering.

  We believe it would be natural to say that the harvesting efficiency of such an array is, at best, 50%. At this stage, we can anticipate a point that, at least in our opinion, is crucial for realistically assess potentialities of rectennas in the field of solar harvesting.

Optics EXPRESS

In Refs. [40] and [41], antennas performance was estimated by resorting to the transmitting efficiency (see Eq. (2) below), namely to the ratio between the power radiated by the antenna vs. the power that is accepted by the antenna itself. For the ideal case we just mentioned, i.e. in the absence of ohmic losses in the antenna, such definition would yield a 100% antenna efficiency. The discrepancy with the intuitive figure of 50% we mentioned above arises from the difference that exists between the concepts of antenna efficiency for transmitting and receiving antennas, respectively. We will discuss the point in more details below.

- Property 2. The receiving area of an array of antennas with ground-plane and matched loads can equal its physical size [49].

  In practical terms, the ensemble of these two properties can be summarized as follows: only in the presence of a ground-plane all the energy incident upon the array can be absorbed by matched loads. This result is of paramount importance for the application we are considering here, where the ultimate goal is the maximization of receiving efficiency of solar radiation.

Dual polarization operations. As a final remark on the proposed periodically loaded surface, we highlight that it easily allows for dual polarization since its geometrical shape is invariant by 90 degrees rotation.

3. Estimation of the harvesting efficiency

In this section we discuss the numerical procedure used to compute the harvesting efficiency of periodically loaded surface in Fig. 1. We report to the figure of merit proposed in Ref. [40], namely the total harvesting efficiency:

$$\eta_{TOT} = \frac{\int_0^\infty d\lambda P(\lambda)\eta_A(\lambda)}{\int_0^\infty d\lambda P(\lambda)} \tag{1}$$

where P(λ) is the Power Spectral Density (PSD) of the incoming sunlight, and $\eta_A(\lambda)$ is the antenna spectral efficiency, respectively. In contrast to Ref. [40], in the present paper:

1. the PSD of real solar spectrum at sea level is considered, as given by the AM1.5 Direct International standard [50] (see the blue curve in Fig. 3) instead of Planck's law of blackbody radiation;

2. most importantly, $\eta_A(\lambda)$ is the receiving rather than transmitting antennas' efficiency. This is the key point we briefly mentioned above and some detailed comments are now worth. In Refs. [40] and [41] the following definition of antenna efficiency was used:

$$\eta_{A,TX}(\lambda) = \frac{P_{rad}(\lambda)}{P_{rad}(\lambda) + P_{loss}(\lambda)} \tag{2}$$

Efficiency was computed as the ratio between the amount of power radiated by the antenna $P_{rad}(\lambda)$ vs. the power that is accepted by the antenna itself ($P_{rad}(\lambda) + P_{loss}(\lambda)$). By contrast, we use here the following definition:

$$\eta_{A,RX}(\lambda) = \frac{P_{LOAD}(\lambda)}{P_{INCIDENT}(\lambda)} \tag{3}$$

According to Eq. (3), the efficiency is defined as the ratio between the power delivered to the load vs. the incoming power. In the case of a periodic structure as our periodically loaded

Optics EXPRESS

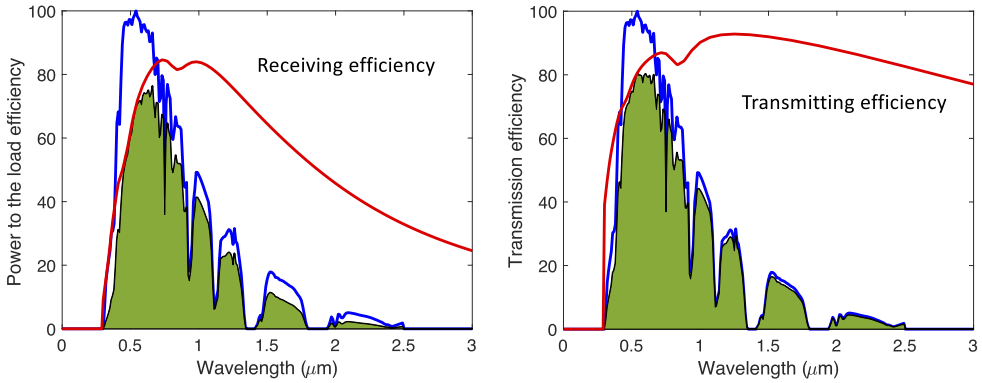

Fig. 3. Example of the results used to optimize the periodically loaded surface of Fig. 1. The blue curve is the solar PSD [50]. In the left panel of the Figure, the red curve is the receiving antenna spectral efficiency $\eta_{A,RX}(\lambda)$. The product between these two curves delimits the green-filled region. The ratio between the areas of the green-filled region, and the region below the blue curve gives the total harvesting efficiency. In the right panel of the Figure, the red curve is the transmitting efficiency.

surface, the incoming power is the amount of power that sunlight carries on the elementary cell of the periodic lattice (see the dashed line in Fig. 1).

Let us highlight the difference between the two definitions. Equation (2) is the definition of antenna efficiency that is customarily employed for antennas used as transmitters. Often, it is also referred to as radiating efficiency (see Ref. [48], Section 11.5) or conduction-dielectric efficiency (see Ref. [51], Section 2.14). It expresses the ratio of the power radiated to the power input of the antenna. In equivalent terms, it also expresses the ratio between the antenna gain and directivity (see Ref. [48], Section 2.15).

In solar harvesting, however, antennas are used as receiving rather than transmitting devices. For a receiving antenna, the concept of equivalent areas is usually employed to describe the power capturing characteristics of the antenna when a wave impinges on it (see Ref. [51], Section 2.15.2). Typically, receiving antennas are characterized by their capture area, defined as the equivalent area, which when multiplied by the incident power density gives the total power captured, i.e. collected (transferred to the antenna load), scattered, or dissipated by the receiving antenna. The following general rule applies (Ref. [51], Section 2.15.2):

$$Capture\ Area = Effective\ Area + Scattering\ Area + Loss\ Area \tag{4}$$

Here the effective area is the ratio of the available power at the antenna's load terminals to the power flux density of a plane wave incident on the antenna, the scattering area is the equivalent area, which, when multiplied by the incident power density, is equal to the scattered or re-radiated power, and the loss area is the equivalent area, which when multiplied by the incident power density leads to the power dissipated as heat in the antenna itself. It is easily seen that the definition of antenna efficiency we use in the present paper, Eq. (3), is related to the antenna capture area as follows:

$$\eta_{A,RX}(\lambda) = \frac{P_{LOAD}(\lambda)}{P_{INCIDENT}(\lambda)} = \frac{EffectiveArea(\lambda)}{CaptureArea(\lambda)} \tag{5}$$

At this stage, a simple and practical comparison between Eq. (2) and Eq. (3) is worth. Let consider once more the case of the ideally lossless and matched antenna we had introduced above. In that case, 100% efficiency would be obtained in (2) : all the power entering into the antenna

Optics EXPRESS

would be radiated. However, the same efficiency is not necessarily obtained in the receiving case (Eq. (3)). In fact, the scattering area, i.e. the amount of power that is "lost" to scattering needs to be considered in the receiving case. As we have recalled above, if the antenna has no back-reflector, the amount of scattered power is at least as large as the power that is transferred to the load. The two powers equal each other if the load impedance is matched. In that case, the receiving efficiency amounts to a maximum 50%, the figure we had previously said we would naturally expect in this case. Only when a back-reflector is added to the antenna the scattered power can be completely canceled out, and 100% receiving efficiency can be obtained.

We summarize the present session with the following general remark: Eq. (2) over-estimates the antenna efficiency as it overlooks the power lost to scattering when the antenna is used as a receiving device. For antennas without back-reflectors, the over-estimation is by a factor of 2 at minimum if the antenna and load impedances are matched, and possibly larger than 2 in the absence of matching.

4. Optimization of receiving efficiency in the periodically loaded surface of Fig. 1

A thorough numerical optimization of the periodically loaded surface in Fig. 1 has been conducted numerically. Results have been cross checked by using two commercial frequency domain Finite Elements Method (FEM) codes (HFSS [52] and Comsol [53]), along with an one in-house Finite-Difference Time-Domain (FDTD) routine. The single elementary cell of the periodically loaded surface (see the dashed line in Fig. 1) was enclosed within periodic boundary conditions. A plane wave was injected from top of the structure. In a first set of simulations, the plane wave was linearly polarized along either the x or y axis in Fig. 1, and it propagated normally to periodically loaded surface (that is, with the incidence angle θ=0, see Fig. 1). Later on, both the azimuthal angle θ and the polar angles ϕ were varied, and a generic elliptic polarization state of the incoming plane wave was used. Loads (red shapes in Fig. 1) were modeled as purely resistive components, with resistance R_L. Loads were connected at the bottom side of the antenna, i.e. they laid on the $\epsilon_r = 2.25$ substrate and they were placed in physical contact with the antenna patches. Numerically, loads were modeled as lumped ports (Comsol [53], HFSS [52]) or lumped RLC boundaries (HFSS [52]), or yet as 1nm thick layers of conducting material (Comsol [53]: transition boundary conditions, HFSS [52]: block material with assigned conductivity). In FDTD modeling, loads were modeled as conducting blocks (with a minimum grid thickness of 4 nm). In all cases, calculation of load delivered to the power was done by numerically evaluating the voltage drop V_L at the load terminals, and then computing power as $P_L = |V_L|^2/(2R_L)$. When using the lumped port modeling, the power to the load could also be evaluated by resorting to the scattering parameter $|S_{21}|$ between the plane wave port and the resistive lumped port. No appreciable differences in computed efficiencies were observed when changing the numerical model for the loads. When we performed the simulations with linearly $x-$ or $y-$polarized electric field impinging on the antennas from normal directions, symmetries could be exploited to reduce the size of the computational domain. This way, the number of elements needed to mesh the domain was in the order of $\sim$ 120.000, with minimum element size <5 nm for the top load and antenna surfaces. Power reflected to the bistatic direction, and the power dissipated in the antenna metallic patches and the back-reflector were also computed. Two materials for antennas and reflector were chosen, and different combinations of materials were tested. Following results from Ref. [40], only aluminum, gold, and silver were considered. Six parameters were then spanned: the lattice pitch Λ, the height H_A and width L_A of the antennas, the thickness H_{diel} of the dielectric substrate, the width W_L and the resistance R_L of the loads.

For any set of spanned parameters, curves like those in Fig. 3 and Fig. 4, as well as contour plots like in Fig. 5 were computed. In Fig. 3, the blue curve is the AM1.5 solar PSD [50]. In the left panel of the Figure, the red curve is the percentage of incoming power that is transferred to the load, i.e. the receiving antenna spectral efficiency $\eta_{A,RX}(\lambda)$ of Eq. (3). The product of the two

Optics EXPRESS

curves gives the green-filled region. The ratio between the area of the green-filled region and the area below the blue curve gives the total harvesting efficiency (Eq. (1)) [40]. In the right panel of the Figure, the red curve is the transmitting efficiency, i.e. the efficiency we have computed through Eq. (2) by assuming that the loads in Fig. 1 were replaced by lumped ports and that power were injected into the antennas through those ports.

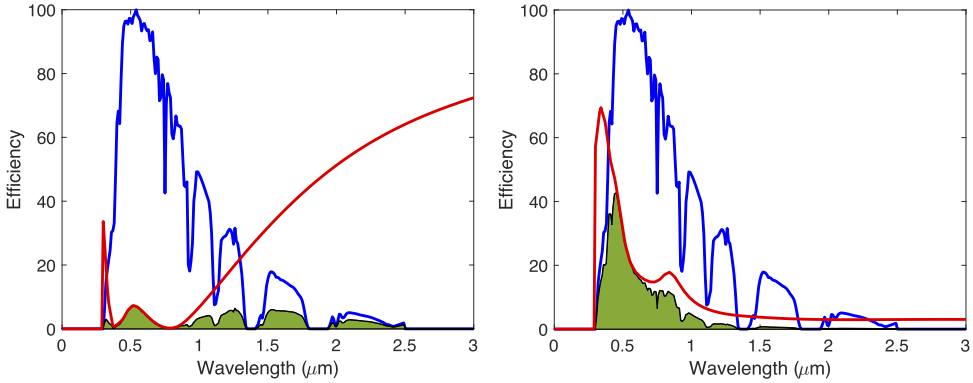

Fig. 4. Similar to Fig. 3, the figure shows examples of the results used to optimize the periodically loaded surface of Fig. 1. In both the panels, the blue curve is the solar PSD [44]. The red curve is the percentage of power that is reflected (left panel) or dissipated (right panel) by antennas in the lattice. The product between these two curves delimits the green-filled region. The ratio between the areas of the green-filled region, and the region below the blue curve gives the total percentage of power that is reflected (left panel) or absorbed (right panel).

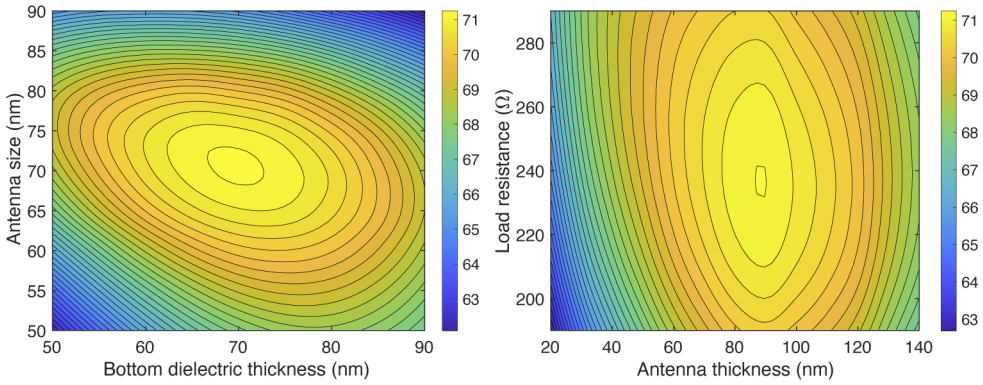

Fig. 5. Left panel. Numerically estimated total harvesting efficiency vs. antenna length/width and substrate dielectric thickness for a lattice with lattice pitch $\Lambda = 140$ nm, load width $W_L = 40$ nm, load resistance $R_L = 236\Omega$, antenna thickness $H_A = 90$ nm. Right panel: Numerically estimated total harvesting efficiency vs. load resistance and antenna thickness for a lattice with lattice pitch $\Lambda = 140$ nm, load width $W_L = 40$ nm, antenna length/width: $L_A = 72$nm, bottom dielectric thickness $H_{diel} = 71$ nm. In both the panels, material used for antennas and substrate were aluminum and gold, respectively.

Similar results are shown in Fig. 4. In the left and right panel of this figure the percentage of power that is reflected or dissipated in the metallic part of the periodically loaded surface are show, respectively. The green filled regions in both the panel allows to compute the cumulative

Optics EXPRESS

reflected and dissipated power, as averaged over the AM1.5 Direct International standard [50] solar PSD.

The following set of parameters was found to provide the largest percentage of power transferred to the load:

- Material for antenna and substrate: aluminum and gold, respectively
- Lattice pitch: $\Lambda = 140$ nm;
- Antenna width: $L_A = 72$ nm;
- Antenna thickness: $H_A = 90$ nm;
- Dielectric substrate thickness: $H_{diel} = 71$ nm;
- Load width: $W_L = 40$ nm;
- Load resistance: $R_L = 236\ \Omega$;

When averaging over the AM1.5 solar spectral distribution, load, reflected and dissipated power percentages equal to 71,2%, 8.8% and 20%, respectively, were found in the receiving case. By contrast, efficiency was $\sim 80\%$ in the transmitting case, leaving a $\sim 20\%$ power loss due to dissipation in the metallic parts of the structure (antennas and back-bacrflector). These values reconfirm the statement we made at the end of Section 3. Transmitting efficiency does not allow to estimate correctly the performance of an antenna aimed at receiving a radiation. In fact, the transmission efficiency can not distinguish between the amount of radiation that is effectively transferred to the load from the radiation that is scattered in the receiving process. In fact, transmission efficiency is larger than receiving efficiency because transmission efficiency is given by the ratio between radiated power and sum of radiated power plus dissipated power (see Eq. (2)). By contrast, receiving efficiency Eq. (3) is the ratio between power transferred to the load and sum of power transferred to the load plus dissipated power plus scattered power. The amount of power transferred to the load in a receiving antenna closed on a perfectly matched load equals the transmitted power of a transmitting antenna fed by a matched generator. Dissipated powers also equal each other in transmitting and receiving antenna under ideal matching conditions. The main difference between transmitting and receiving efficiency depends therefore on scattered power, which is accounted for in Eq. (3), and neglected in Eq. (2). As a consequence, Eq. (2) over-estimates the real receiving efficiency of the antenna. Recall that in the absence of a back-reflector, the scattered power can be even larger than the power transferred to the load, and so the over-estimation can be high, especially in absence of matching between the antenna and load impedances. A few comments are in order.

- First of all: 71.2% is the main result of the present paper. We remark once more that this is a receiving efficiency, that is percentage of power that is really transferred from sunlight to the antennas' loads (under normal illumination). Also, this result was checked to hold for any state of polarization of the incoming light. This is expected because any polarization state can always be decomposed into a combination of linear x and y states (see the Cartesian frame in Fig. 1), possibly with a phase mismatch. Power transfer to loads, however, is phase independent, and the geometrical shape of loads and antennas causes the part of power that is not absorbed along the x-axis to be absorbed along the y-one, and vice-versa. At the best of our knowledge, this is the largest receiving efficiency ever estimated so far for unpolarized light.
- The left panel of Fig. 4 shows a result analogous to that of Fig. 3, but now for the power that is reflected, i.e. scattered, by the periodically loaded surface. The red curve in the figure

Optics EXPRESS

shows that a small amount of power is reflected in the visible spectrum wavelengths, while severe reflection occurs for wavelengths beyond $\sim 2\,\mu$m. However, when the reflection curve is averaged over the AM1.5 solar spectrum, a very limited overall (8.8%) reflection is found. Similar curves are finally shown in the right panel of the figure for the power dissipated in the antennas. When the dissipation curve is averaged over the AM1.5 solar spectrum, an overall 20% dissipation value is found.

If the computation were restricted to the wavelengths of the visible range, a $\sim 4\%$ reflection would be obtained. We remark once more that the presence of the back-reflector plays a crucial role in the reduction of reflection, as it was proved experimentally in a lattice of gold dipole antennas on top of a gold reflector [54].

- It is worth mentioning that further refinement and optimization of the geometry would lead to sligthly higher efficiency: shaping properly the patch section with respect the z direction, and adjusting the z-position of the metal with respect to the dielectric slab, could lead to an efficiency higher than 75%. In this work, we just avoided to consider such extra-complicated solutions.

  Also, we numerically verified that the efficiency did not change to within a tenth of percent if the aluminum antenna were coated with a 1nm thin layer of aluminum oxide.

- Finally, we remark some interesting features that can be inferred by looking at the difference between the left and right panels of Fig. 3, that is between receiving and transmitting efficiencies. The two curves are almost identical for wavelength smaller than $\simeq 1\mu$m, and remarkably different for wavelengths larger than $\simeq 1\mu$m. Recall that the receiving curve is shown for a resistive load $R_L = 236\,\Omega$. Whereas, source impedance is assumed to be perfectly matched to the antenna impedance in the transmitting case. By inspecting the left panel of Fig. 2, one may recognize the effect of poor load matching in the receiving case. When wavelengths smaller than $\simeq 1\mu$m, the imaginary part of the lattice load is almost null, and its real part close to $236\,\Omega$. Whereas, lattice resistance starts to reduce for λ>1 μm, and a reactive component starts to appear, causing poor matching with the load. Consistently, reflection from the lattice increases (see left panel of Fig. 4).

The contour plots of Fig. 5 show the dependence of the antenna efficiency on variations of geometrical dimensions around the optimum value. For instance, the efficiency vs. antenna size 50 nm < L_A < 90 nm and dielectric substrate thickness 50 nm < H_{diel} < 90 nm is shown in the left panel of the figure. Optimum values listed above were used for lattice pitch, load resistance and width, and antenna thickness. In a similar fashion, the right panel of the figure shows the estimated efficiency variation vs the antenna thickness and load resistance. In this case too other parameters were set to be the optimum ones.

Figure 6 shows the dependence of the efficiency on the load impedance. In the left panel of the figure, a purely resistive load is considered, and the efficiency vs. load resistance is shown for a lattice having the optimum parameters listed above. As previously mentioned, the largest performance leading to $\sim 71\%$ efficiency is observed for load resistances $R_L \approx 236\Omega$, while efficiency values larger than 50% are still obtained for R_L in the range between ~ 100 to $\sim 1000\Omega$. In the right panel of the figure, we show an example of how the efficiency worsens when the load is no longer purely resistive. Figure refers to the case of a parallel RC load, with $R = 50, 236$ and $1000\,\Omega$ for light blue, red and black curves, respectively. We remark that a precise computation of the effect of a generic load $Z_L(\lambda)$ on the antenna efficiency cannot be done *rigorously* because the field that is back-scattered by the antenna depends on the load itself. In other words, only a numerical computation could allow to determine exactly how much of the incoming field is scattered and how much is transferred to the load.

Optics EXPRESS

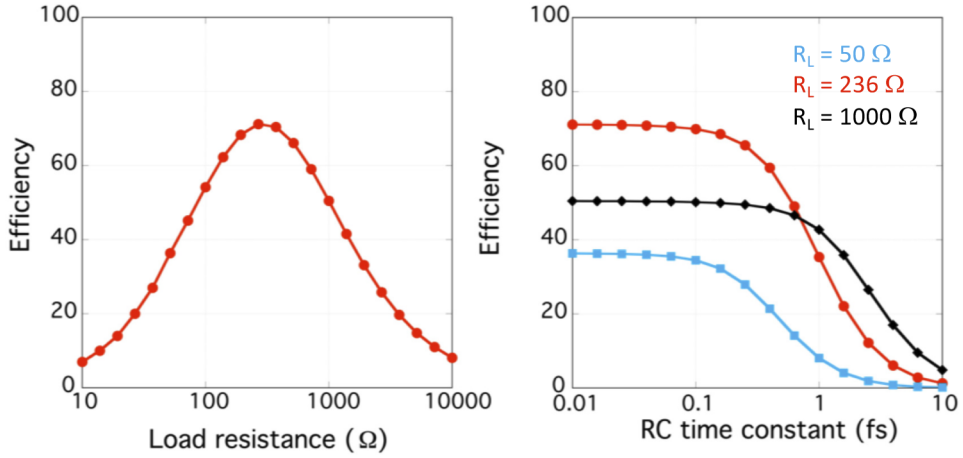

Fig. 6. Left panel. Numerically estimated total harvesting efficiency vs. load resistance for the optimized lattice with the following parameters: lattice pitch $\Lambda = 140$nm, load width $W_L = 40$ nm, antenna length/width: $L_A = 72$ nm, antenna thickness $H_A = 90$ nm, bottom dielectric thickness $H_{diel} = 71$ nm. Right panel. Numerically estimated efficiency for a parallel RC load. Light blue, red and black curves refer to load resistance equal to 50, 236 and 1000 Ω, respectively.

An approximate computation can be done as follows. Any receiving antenna can be regarded as a voltage generator with assigned open circuit voltage $V_0(\lambda)$ and internal resistance $Z_A(\lambda)$, closed on a load with impedance $Z_L(\lambda)$. The amount of real power that is transferred to the load is $P_{LOAD}(\lambda) = |V_0(\lambda)|^2 ReZ_L(\lambda)/|Z_L(\lambda) + Z_A(\lambda)|^2$. Using this expression in Eqs. (3) and (1), along with the antenna internal impedance $Z_A(\lambda)$ shown in the left panel of Fig. 2 an estimation of the harvesting efficiency for any generic load $Z_L(\lambda)$ can be obtained.

In both the panels, performance drop with respect to the ideal and optimum case of purely resistive load having $R_L = 236\,\Omega$ is due to the mismatch between the antenna and load impedances. In particular, in the right panel of the figure, the load is short-circuited for increasing values of the RC time constant, and very little real power is transferred to the resistive component of the load.

Finally, Fig. 7 shows the estimated harvesting efficiency as a function of the angle of incidence of impinging radiation (that is, as a function of the azimuthal angle of a polar coordinate system centered on the elementary cell of the lattice). In the left panel of the figure, spectral efficiency is shown for angle of incidence $\theta_i = 0$ degrees (black line), $\theta_i = 20$ degrees (red line), $\theta_i = 40$ degrees (blue line) (red line), and $\theta_i = 60$ degrees (green line), respectively. A reduction of efficiency for increasing angle of incidence is observed, along with a shift towards longer wavelengths (where the solar spectrum content is poor). In the right panel of the figure, the overall receiving efficiency averaged over the AM1.5 solar spectrum is shown (red curve). A fairly smooth dependence on the angle of incidence is observed. Efficiency remains larger than 60% up to 35 degrees, and larger than 50% up to 50 degrees. Percentages of power dissipated in the metallic parts of the lattice (black line) and power reflected n the bistatic direction (blue line) are also shown in the figure. Similar to the case of the receiving efficiency (red curve), also dissipated and reflected efficiencies are averaged over the AM1.5 solar spectrum.

Optics EXPRESS

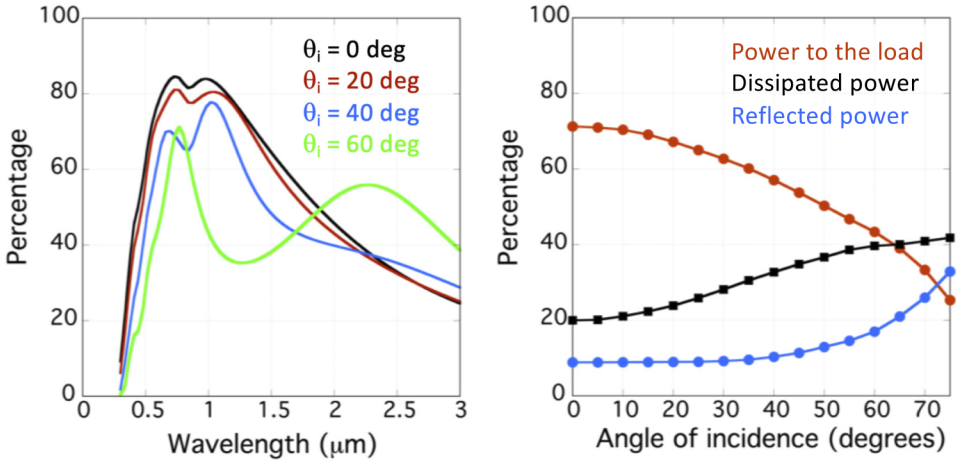

Fig. 7. Left panel. Receiving efficiency curves for light impinging on the array of loaded resonators with the angle of incidence $\theta_i = 0$ degrees (black line), $\theta_i = 20$ degrees (red line), $\theta_i = 40$ degrees (blue line) (red line),and $\theta_i = 60$ degrees (green line), respectively. Right panel: Dependence of the total harvesting efficiency (red curve), power dissipated in metallic parts of the lattice (black curve) and reflected power (light blue curve) for the optimized lattice vs the angle of incidence of incident light.

5. Estimation of voltage drop at terminals of the antennas' loads

We previously underlined that antenna loads have been assumed here to be simple resistors, while rectifying diodes will be required in real applications. We did not speculate in this paper on how diodes will be fabricated, nor on which physical effect their rectification capabilities will ground. Yet, we believe it is worth to give an estimate of the magnitude of the voltage drop those diodes will be presented at their terminals when the sunlight illuminates the antenna array. To give such estimate, we first evaluate the upper limit to the voltage drop, i.e. the voltage magnitude that we would find if the sunlight could be completely absorbed by the array. Later on, we compare this upper limit with realistic values obtained by the lattice with optimum parameters as in the previous section.

Let us assume initially that the following ideal conditions apply:

1. the loads connecting neighboring antennas (red shapes in Fig. 1) matches perfectly the antenna internal impedance R_i at all frequencies;
2. the effective area of each antenna equals the geometrical area of the unit cell; that is: antennas are lossless, their orientation is optimal with respect to the incoming light, and depolarization factor is unitary so that all the incoming power is delivered to the loads.

Under these conditions, the receiving antenna effective length is [48]:

$$\mathbf{h}_{RX} = 2\sqrt{\frac{R_i A_{eff}}{Z_0}} = 2\sqrt{\frac{R_i A_{geom}}{Z_0}} = 2\Lambda\sqrt{\frac{R_i}{Z_0}} \tag{6}$$

where $Z_0 = 120\pi$ is the wave impedance in vacuum. Keeping in mind that optimal antenna orientation has been assumed, as well as that the antenna internal impedance is matched to the

Optics EXPRESS

load, the voltage drop at load terminals is:

$$V_{load}^{max} = \frac{\mid \mathbf{E}_i \cdot \mathbf{h}_{RX} \mid}{2} = \frac{\mid \mathbf{E}_i \mid \cdot \mid \mathbf{h}_{RX} \mid}{2} = \Lambda \mathbf{E}_i \sqrt{\frac{R_i}{Z_0}} \tag{7}$$

Here $\mid \mathbf{E}_i \mid$ is the amplitude of the incoming electric field. Superscript "max" has been added to remind that this is the largest voltage load that the array could provide under the ideal conditions listed above.

In the case of solar illumination, the incoming electric field is the superposition of waves with different frequencies, having the PSD given by the blue curve in Fig. 3 [50].

Computation of the amplitude of the electric field due to the whole solar spectrum can be done as follows. We divide the PSD into slices sampled over a given set of wavelengths. Then, we convert the solar PSD:

$$PSD(f)\Delta f = PSD(\lambda)\Delta\lambda \Longrightarrow PSD(f) = PSD(\lambda)c_0/f^2 \tag{8}$$

Given that the sunlight is unpolarized, half of the PSD is assigned to each of two orthogonal polarizations. For each of them, the amplitude of the electric field within each slice of the PSD is given by

$$\frac{\mid \mathbf{E}_i{}^{sun} \mid^2}{2Z_0} = \frac{PSD(f_k)}{2}\Delta f_k \tag{9}$$

with f_k and Δf_k the central frequency and the bandwidth of the k-th slice, respectively. Electric field due to solar radiation therefore is, for each of two orthogonal polarizations:

$$\mathbf{E}_{tot}{}^{sun}(t) = \sum_k \sqrt{Z_0 PSD(f_k)\Delta f_k} cos(2\pi f_k t + \phi_k) \tag{10}$$

with ϕ_k a $[0,2\pi]$ uniformly distributed random variable accounting for spectral incoherence. From Eq. (7), the voltage drop at the antenna terminals turns out to be:

$$V_{load}^{max} = \sum_k \frac{\mid \mathbf{E}_i(f_k) \cdot \mathbf{h}_{RX}(f_k) \mid}{2} = \sum_k \mid \mathbf{E}_i{}^{sun}(f_k) \mid \Lambda \sqrt{\frac{R_i(f_k)}{Z_0}} = \sum_k \Lambda \sqrt{R_i(f_k) PSD(f_k)\Delta f_k} \tag{11}$$

where we have used the assumption that under ideal conditions the antenna effective length is constant (and equal to its maximum attainable value, see Eq. (6)) at all frequencies. Once more, we remark that the result holds for each orthogonal polarization. Each spectral component contributes to the total RMS voltage with the term:

$$(V_{RMS,k}^2)^{max} = \frac{1}{2\pi}\int \Lambda^2 R_i(f_k) PSD(f_k)\Delta f_k cos^2(x)dx = \frac{\Lambda^2 R_i(f_k) PSD(f_k)\Delta f_k}{2} \tag{12}$$

For each of two orthogonal polarizations, the total RMS voltage at the load terminals thus is:

$$V_{RMS}^{max} = \sqrt{\sum_k (V_{RMS,k}^2)^{max}} = \frac{\Lambda}{\sqrt{2}} \sqrt{\sum_k R_i(f_k) PSD(f_k)\Delta f_k} \tag{13}$$

For the sake of simplicity in the calculation, we assume that the lattice resistance is independent of frequency, with a value equal to the optimum we found in the preceding section: $R_i = 236\Omega$. Also, $\Lambda = 140$nm, so that $V_{RMS}{}^{max} \approx 45\mu V$ is numerically found from 13 for the AM1.5 solar spectrum [50].

We now turn to the evaluation of voltage drop at load terminals in a realistic antenna where both losses of metals and matching between internal antenna impedance and load are taken into

Optics EXPRESS

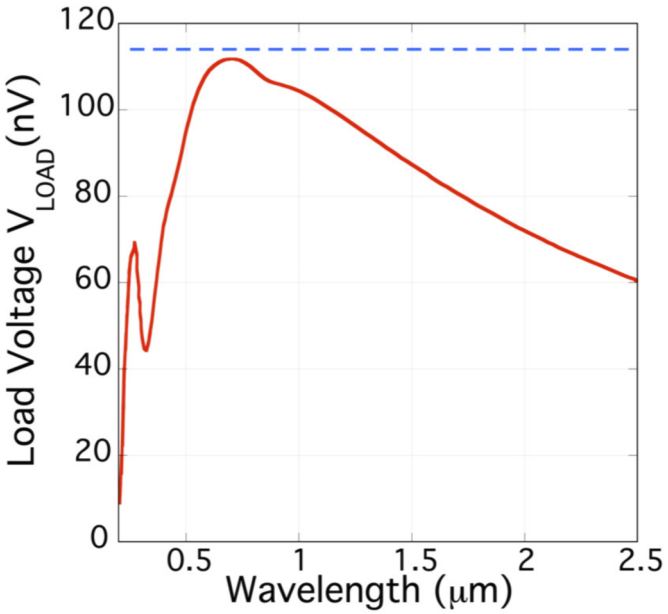

Fig. 8. Numerically computed voltage across a $R_L = 236\Omega$ resistance load for the optimized antenna array, for an $|\mathbf{E}_i|$=1V/m incident electric field. The dashed blue line is the upper limit for the load voltage, as computed by assuming that the antenna impedance matches the load at all frequencies, and that the antenna efficiency is unitary.

account. Figure 8 shows the numerically computed voltage drop V_{Load} at the terminals of the array with optimized parameters when the amplitude of the incident field is $|\mathbf{E}_i|$=1V/m at all frequencies. For comparison, in the figure we also plot with dashed blue line the upper limit ${V_{Load}}^{max} = \Lambda\,|\,\mathbf{E}_i\,|\,\sqrt{(R_L/Z_0)} \approx 111nV$ for $\mathbf{E}_i = 1$ V/m.

Similar to computations in Eqs. (10)–(12) above, the total RMS voltage at load terminals due to the whole AM1.5 spectrum, and for each of two orthogonal polarizations, can be evaluated as follows:

$$V_{RMS} = \sqrt{\sum_k (\frac{(|{\mathbf{E}_i}^{sun}(f_k)\,|)}{1V/m} V_{Load}(f_k))^2} \tag{14}$$

Numerically, we found $V_{RMS} \approx 36\mu V$ to be comparewd with ${V_{RMS}}^{max} \approx 45\mu V$. Under normal illumination, and due due polarization insensitiveness of the periodically loaded surface of Fig. 1, this is the RMS voltage that is expected to be found at the terminals of all the four diodes that connect any antenna to neighboring ones.

6. Conclusion

In this paper, a periodically loaded surface has been proposed for harvesting of sunlight. Estimates of harvesting efficiency have been discussed by several authors in recent years [36,40,41]. Yet, the present paper distinguishes from previous one in two main respects. First, we proposed to measure the antenna performance in a different way with respect to previously published papers. In fact, while in existing literature a transmitting efficiency was used, we referred here to receiving efficiency. This was made because, on the one hand, antennas for solar harvesting are receiving devices. On the other hand, as we proved in the paper, transmitting efficiency may greatly over-estimate the real receiving antenna efficiency due to unavoidable scattering of incoming radiation. The second novelty of the present paper is the use of a structure comprising

Optics EXPRESS

an infinite array of closely packed antennas placed over a reflecting mirror instead of a single isolated antenna in free space or over a dielectric slab. Both the array arrangement and the use of a reflector represent a more realistic device for harvesting of sunlight than a single antenna. In fact, close packing of antennas avoids waste of available space. Mirror increases the mechanical robustness of the structure and also constitutes an electrical contact for extracting converted energy. Besides, we have proved that both the array arrangement and the reflector have beneficial effects on efficiency. By using an array with a pitch much smaller than the solar wavelengths, even those in the visible range, a flat frequency response of the antenna impedance was obtained, allowing for matching to the load. In addition, the small array pitch also brought to a fair independence of the harvesting efficiency on the angle of incidence of sunlight. Finally, by using a square lattice, real dual-polarization operation of the array was made possible. Use of mirror allowed to enlarge the antenna effective area and to reduce the scattering area at the same time, finally leading to an extremely efficient power transfer from antennas to loads. We have underlined in the paper that only in the presence of the mirror a 100 % receiving efficiency is theoretically possible, while the ultimate upper bound for antennas without mirror can not exceed 50% due to intrinsic scattering of incoming radiation. By carefully optimizing the geometrical parameters of the proposed periodically loaded surface, a receiving efficiency as high as 71% was obtained. As a side effect of such a large receiving efficiency, we also proved that when averaging over the sunlight spectrum, an overall reflection smaller than 10% is found. The proposed structure behaves as a sort of stealth surface for sunlight, with a 10-fold reduction of the radar cross section in the 300 to 3000 nm range with respect to the reflection from a flat metallic surface.

Funding. Horizon 2020 Framework Programme (101006963).

Acknowledgments. This project has received funding from the European Union's Horizon 2020 research and innovation program under grant agreement No 101006963 (GreEnergy). This document reflects only the view of the authors. The funding agency is not responsible for any use that may be made of the information it contains.

Disclosures. The authors declare no conflicts of interest.

Data availability. Data underlying the results presented in this paper are not publicly available at this time but may be obtained from the authors upon reasonable request.

References

1. B. Sorensen, *Renewable Energy* (Academic Press, 2017).
2. S. Tagliapietra, *Global Energy Fundamentals: Economics, Politics, and Technology* (Cambridge University Press, 2020).
3. B. E. D. Martinez and T. Wagner, *Energy Efficiency* (Elsevier Science, 2019).
4. UN General Assembly, "Transforming our world: the 2030 Agenda for Sustainable Development," 21 October 2015, A/RES/70/1, https://www.refworld.org/docid/57b6e3e44.html.
5. U.S. Energy Information Administration, "What is Energy? Sources of energy," https://www.eia.gov/energyexplained/what-is-energy/sources-of-energy.php.
6. M. A. Lange, *Vulnerability of Energy to Climate* (R. A. Pielke, Academic Press, 2013).
7. W. v. S. A. Reinders and P. Verlinden, *Front Matter* (John Wiley and Sons, Ltd, 2016)., pp. i–xxxv
8. W. S. Keith Lovegrove, *Concentrating Solar Power Technology: Principles, Developments and Applications* (Keith Lovegrove, Wes Stein, 2012).
9. M. Green, "Photovoltaic principles," Phys. E: Low-dimensional Syst. Nanostructures **14**(1-2), 11–17 (2002).
10. K. Yoshikawa, H. Kawasaki, W. Yoshida, T. Irie, K. Konishi, K. Nakano, T. Uto, D. Adachi, M. Kanematsu, H. Uzu, and K. Yamamoto, "Silicon heterojunction solar cell with interdigitated back contacts for a photoconversion efficiency over 26%," Nat Energy **2**(5), 17032 (2017).
11. UN General Assembly, "World Record Solar Cell with 44.7% Efficiency," https://www.ise.fraunhofer.de/en/press-media/press-releases/2013/world-record-solar-cell-with-44-7-efficiency.html.
12. M. A. Green, E. D. Dunlop, J. Hohl-Ebinger, M. Yoshita, N. Kopidakis, and X. Hao, "Solar cell efficiency tables (version 58)," Prog Photovolt Res Appl. **29**, 657-667 (2021).
13. A. E. Elmohlawy, V. F. Ochkov, and B. I. Kazandzhan, "Thermal performance analysis of a concentrated solar power system (csp) integrated with natural gas combined cycle (ngcc) power plant," Case Stud. Therm. Eng. **14**, 100458 (2019).
14. W. C. Brown and R. H. George, "Rectification of microwave power," IEEE Spectrum **1**(10), 92–97 (1964).

Optics EXPRESS

15. W. C. Brown, "The history of the development of the rectenna," in *Rectenna session of the SPS microwave system works, Lyndon B. Johnson Space Center*, (1980), pp. 15–18.
16. R. L. Bailey, "A Proposed New Concept for a Solar-Energy Converter," J. Eng. for Power **94**(2), 73–77 (1972).
17. F. H. Alharbi and S. Kais, "Theoretical limits of photovoltaics efficiency and possible improvements by intuitive approaches learned from photosynthesis and quantum coherence," Renew. Sustain. Energy Rev. **43**, 1073–1089 (2015).
18. A. D. Vos, "Detailed balance limit of the efficiency of tandem solar cells," J. Phys. D: Appl. Phys. **13**(5), 839–846 (1980).
19. R. Corkish, M. Green, and T. Puzzer, "Solar energy collection by antennas," Sol. Energy **73**(6), 395–401 (2002).
20. W. C. Brown, "The receiving antenna and micr0wave power rectification," J. Microw. Power **5**(4), 279–292 (1970).
21. M. Dragoman and M. Aldrigo, "Graphene rectenna for efficient energy harvesting at terahertz frequencies," Appl. Phys. Lett. **109**(11), 113105 (2016).
22. P. Bharadwaj, B. Deutsch, and L. Novotny, "Optical antennas," Adv. Opt. Photonics **1**(3), 438–483 (2009).
23. L. Novotny, "Effective wavelength scaling for optical antennas," Phys. Rev. Lett. **98**(26), 266802 (2007).
24. A. Khalid, N. J. Pilgrim, G. M. Dunn, M. C. Holland, C. R. Stanley, I. G. Thayne, and D. R. S. Cumming, "A planar gunn diode operating above 100 ghz," IEEE Electron Device Lett. **28**(10), 849–851 (2007).
25. D. Georgiadou, J. Semple, A. Sagade, H. Forstén, P. Rantakari, Y.-H. Lin, F. Alkhalil, A. Seitkhan, K. Loganathan, H. Faber, and T. Anthopoulos, "100 ghz zinc oxide schottky diodes processed from solution on a wafer scale," Nat. Electron. **3**(11), 718–725 (2020).
26. B. Eliasson, "Metal-insulator-metal diodes for solar energy conversion," PhD thesis, Graduate School of University of Colorado (2001).
27. B. J. Eliasson and G. Moddel, "Metal-oxide electron tunneling device for solar energy conversion," US Patent 6534784 (18 March 2003).
28. G. Moddel and S. Grover, *Rectenna Solar Cells* (Springer, 2013).
29. C. Fumeaux, J. Alda, and G. Boreman, "Lithographic antennas at visible frequencies," Opt. Lett. **24**(22), 1629–1631 (1999).
30. NGI, National Graphene Institute, The University of Manchester, UK, "Discovery of graphene," https://www.graphene.manchester.ac.uk/learn/discovery-of-graphene/.
31. European Project 101006963, "GreEnergy," https://www.greenergy-project.eu/.
32. Anandtech, "Intel's Manufacturing Roadmap from 2019 to 2029: Back Porting, 7nm, 5nm, 3nm, 2nm, and 1.4 nm," https://www.anandtech.com/show/15217/intels-manufacturing-roadmap-from-2019-to-2029.
33. L. Banszerus, M. Schmitz, S. Engels, M. Goldsche, K. Watanabe, T. Taniguchi, B. Beschoten, and C. Stampfer, "Ballistic transport exceeding 28 μm in cvd grown graphene," Nano Lett. **16**(2), 1387–1391 (2016).
34. Z. Zhu, S. Joshi, S. Grover, and G. Moddel, "Graphene geometric diodes for terahertz rectennas," J. Phys. D: Appl. Phys. **46**(18), 185101 (2013).
35. S. G. Z. Zhu, S. Joshi, and G. Moddel, *Geometric Diodes for Optical Rectennas* (Springer NY, 2013), pp. 209–227.
36. Z. Ma and G. A. Vandenbosch, "Optimal solar energy harvesting efficiency of nano-rectenna systems," Sol. Energy **88**, 163–174 (2013).
37. A. M. Song, P. Omling, L. Samuelson, W. Seifert, I. Shorubalko, and H. Zirath, "Operation of ingaas/inp-based ballistic rectifiers at room temperature and frequencies up to 50 ghz," Jpn. J. Appl. Phys. **40**(Part 2, No. 9A/B), L909–L911 (2001).
38. G. Auton, J. Zhang, R. K. Kumar, H. Wang, X. Zhang, Q. Wang, E. Hill, and A. Song, "Graphene ballistic nano-rectifier with very high responsivity," Nat. Commun. **7**(1), 11670 (2016).
39. V. H. Nguyen, D. C. Nguyen, S. Kumar, M. Kim, D. Kang, Y. Lee, N. Nasir, M. A. Rehman, T. P. A. Bach, J. Jung, and Y. Seo, "Optimum design for the ballistic diode based on graphene field-effect transistors," npj 2D Mater. Appl. **5**(1), 89 (2021).
40. G. A. Vandenbosch and Z. Ma, "Upper bounds for the solar energy harvesting efficiency of nano-antennas," Nano Energy **1**(3), 494–502 (2012).
41. H. Zhao, H. Gao, T. Cao, and B. Li, "Efficient full-spectrum utilization, reception and conversion of solar energy by broad-band nanospiral antenna," Opt. Express **26**(2), A178–A191 (2018).
42. V. Agrawal and Y. Lo, "Mutual coupling in phased arrays of randomly spaced antennas," IEEE Trans. Antennas Propag. **20**(3), 288–295 (1972).
43. B. A. Munk, "Periodic surface for large scan angles," US Patent 3789404A, (16 October 1968.
44. B. A. Munk, *Frequency Selective Surfaces, Theory and Design* (John Wiley and Sons, 2000).
45. B. A. Munk, *Finite Antenna Arrays and FSS* (John Wiley and Sons, 2003).
46. H. A. Wheeler, "Simple relations derived from a phased array antenna made of an infinite current sheet," IEEE Trans. Antennas Propag. **13**(4), 506–514 (1965).
47. A. D. Rakić, A. B. Djurišić, J. M. Elazar, and M. L. Majewski, "Optical properties of metallic films for vertical-cavity optoelectronic devices," Appl. Opt. **37**(22), 5271–5283 (1998).
48. J. Kraus, *Antennas* (New York: McGraw-Hill, 1950).
49. S. A. Schelkunoff and H. T. Friis, *Antenna Theory and Practice* (John Wiley and Sons, 1952).
50. C. Gueymard, D. Myers, and K. Emery, "Proposed reference irradiance spectra for solar energy systems testing," Sol. Energy **73**(6), 443–467 (2002).

Optics EXPRESS

51. C. A. Balanis, *Antenna Theory*, 3rd Ed. (John Wiley and Sons, 2005).
52. "Ansys HFSS," https://www.ansys.com/it-it/products/electronics/ansys-hfss.
53. Comsol, Inc., "Comsol - Software for Multiphysics," https://www.comsol.com/.
54. T. J. Seok, A. Jamshidi, M. Kim, S. Dhuey, A. Lakhani, H. Choo, P. J. Schuck, S. Cabrini, A. M. Schwartzberg, J. Bokor, E. Yablonovitch, and M. C. Wu, "Radiation engineering of optical antennas for maximum field enhancement," Nano Lett. **11**(7), 2606–2610 (2011).